



Observation of a uniaxial ferroelectric smectic A phase

Xi Chen^a🗓 , Vikina Martinez^a, Pierre Nacke^b, Eva Korblova^c🗓 , Atsutaka Manabe^d, Melanie Klasen-Memmer^d, Guillaume Freychet^e🗓 , Mikhail Zhernenkov^e, Matthew A. Glaser^a, Leo Radzihovsky^a, Joseph E. Maclennan^a, David M. Walba^c, Matthias Bremer^d, Frank Giesselmann^b, and Noel A. Clark^{a,1}

Contributed by Noel Clark; received June 27, 2022; accepted October 13, 2022; reviewed by Nicholas Abbott and Peter Palffy-Muhoray

We report the observation of the smectic A_F, a liquid crystal phase of the ferroelectric nematic realm. The smectic A_F is a phase of small polar, rod-shaped molecules that form two-dimensional fluid layers spaced by approximately the mean molecular length. The phase is uniaxial, with the molecular director, the local average long-axis orientation, normal to the layer planes, and ferroelectric, with a spontaneous electric polarization parallel to the director. Polarization measurements indicate almost complete polar ordering of the ~10 Debye longitudinal molecular dipoles, and hysteretic polarization reversal with a coercive field $\sim 2 \times 10^5$ V/m is observed. The SmA_F phase appears upon cooling in two binary mixtures of partially fluorinated mesogens: 2N/DIO, exhibiting a nematic (N)-smectic Z_A (SmZ_A)-ferroelectric nematic (N_F)-SmA_F phase sequence, and 7N/DIO, exhibiting an N-SmZ_A-SmA_F phase sequence. The latter presents an opportunity to study a transition between two smectic phases having orthogonal systems of layers.

liquid crystal | ferroelectric | smectic | nematic

Proper ferroelectricity in liquids was predicted in the 1910s by P. Debye (1) and M. Born (2), who applied the Langevin-Weiss model of ferromagnetism to propose a liquid-state phase change in which the ordering transition is a spontaneous polar orientation of molecular electric dipoles. A century later, in 2017, two groups independently reported, in addition to the typical nematic (N) phase, novel nematic phases in strongly dipolar mesogens, the "splay nematic" in the molecule RM734 (3-5), and a "ferroelectric-like nematic" phase in the molecule DIO (6). These nematic phases were subsequently demonstrated to be ferroelectric in both RM734 (7) and in DIO (8, 9) and to be the same phase in these two materials (9). This new phase, the ferroelectric N (N_F) , is a uniaxially symmetric, spatially homogeneous, N liquid having ≥90% polar ordering of its longitudinal molecular dipoles (7, 9). A related new phase recently observed is the helical N_F (10-14), obtained by chiral doping of RM734, DIO, or their homologs or by introducing chiral tails into the molecular structures (15). DIO also exhibits an additional phase, found between the N and N_F (6), which we have recently characterized, terming it the smectic Z_A (16) and showing it also to be new: a density-modulated antiferroelectric exhibiting lamellar order with ~18 nm repeats, comprising pairs of ~9-nm-thick layers with alternating polarization, the director and polarization being oriented parallel to the layer planes.

Here, we introduce another phase of the N_F realm, a uniaxial, lamellar phase with the director normal to the layers and a spontaneous polarization along the director, which we have termed the SmA_F (17, 18). Schematic drawings of the phases discussed here, sorted into macroscopically nonpolar and polar types, are shown in Fig. 1, along with the molecular structures and phase sequences of the mesogens used in the mixtures. The macroscopically nonpolar, paraelectric N and smectic A (SmA) phases, the N_F and ferroelectric SmA (SmA_F) phases, and the antiferroelectric SmZ_A phase are sketched in Fig. 1A, the light-to-dark shading of the schematic molecules indicating their dipolar symmetry. The SmA_F phase is observed in 50:50 wt% AUUQU2N/DIO (2N/DIO) and AUUQU7N/DIO (7N/DIO) mixtures. The region of Fig. 1A shaded yellow shows the generic phase sequence observed in the mixtures on cooling (Iso \rightarrow $N \to SmZ_A \to N_F \to SmA_F \to X$), noting that some phases may be missing in a given component or mixture. For example, none of the single components exhibits the SmA_F phase, and the 7N/DIO mixture does not have the N_F phase. The first mesophase that appears on cooling any of the components and mixtures from the isotropic is the conventional dielectric N phase, which, in the present context, is also considered paraelectric. They all cool from the N into the antiferroelectric smectic Z (SmZ_A) (16) phase.

The 2N/DIO mixture then transitions first to the N_F phase and then, on further cooling, to the SmA_F, while 7N/DIO goes directly to the SmA_F. This enables a comparative study of the $N_F \to SmA_F$ and $SmZ_A \xrightarrow{-} SmA_F$ transitions, the latter entailing the simultaneous disappearance of the SmZ_A layering parallel to the director and the formation of the SmA_F layering normal to the director, in the absence of any director/polarization reorientation.

Significance

Liquid crystal science grows in richness and applicability with each new phase that is found or created. The recent discovery of the ferroelectric nematic was both thrilling and unexpected, since it appeared in new molecules not much different in structure from many similar materials studied over the last 100 years. Clearly, significant secrets remain to be discovered in the complexities of organic molecular architecture and interaction. A fundamental question following the ferroelectric nematic discovery was whether there could also be a ferroelectric smectic A, the nematic-companion phase obtained when molecules spontaneously position to form planar, fluid layers normal to their molecular long axes. Here, we report such a phase, broadening the ferroelectric nematic realm.

Author contributions: X.C., V.M., P.N., E.K., M.K.-M., G.F., M.Z., M.A.G., J.E.M., D.M.W., M.B., F.G., and N.A.C. designed research; X.C., V.M., P.N., E.K., M.K.-M., G.F., M.Z., M.A.G., L.R., J.E.M., M.B., F.G., and N.A.C. performed research; E.K., A.M., M.K.-M., D.M.W., and M.B. contributed new reagents/analytic tools; X.C., V.M., P.N., M.A.G. I.EM. F.G. and N.A.G. capalyzed data: and X.G. M.A.G., J.E.M., F.G., and N.A.C. analyzed data; and X.C., J.E.M., and N.A.C. wrote the paper.

Reviewers: N.A., Smith School of Chemical and Biomolecular Engineering, Cornell University; and P.P.-M., Kent State University.

The authors declare no competing interest.

Copyright © 2022 the Author(s). Published by PNAS. This article is distributed under Creative Commons Attribution-NonCommercial-NoDerivatives License 4.0 (CC BY-NC-ND).

¹To whom correspondence may be addressed. Email: noel.clark@colorado.edu.

This article contains supporting information online at http://www.pnas.org/lookup/suppl/doi:10.1073/pnas. 2210062119/-/DCSupplemental.

Published November 14, 2022.

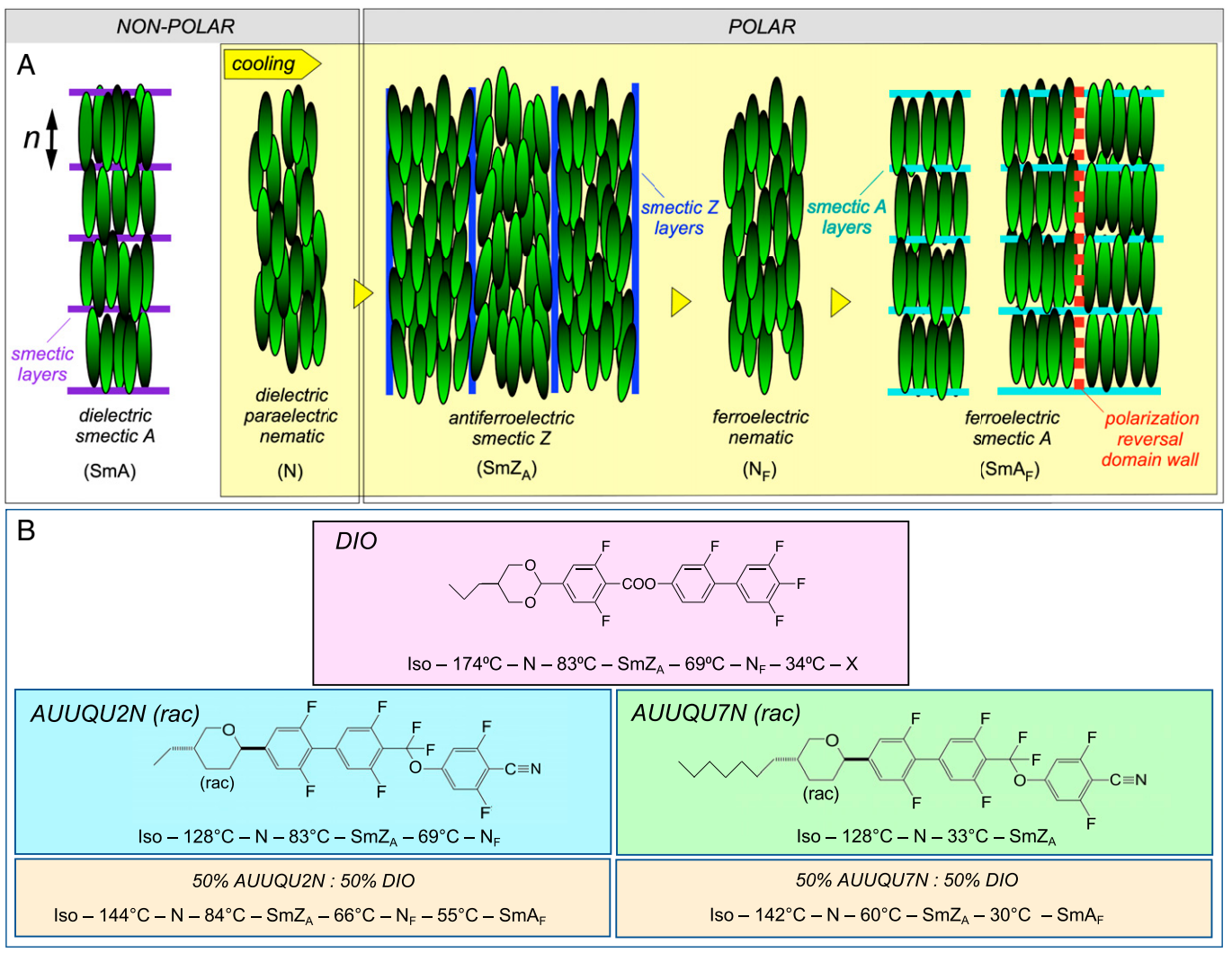


Fig. 1. Structures, phase sequences, and schematic of the liquid crystal phase behavior of 2N, 7N, and DIO single components and their indicated mixtures. (A) The relevant phases of rod-shaped molecules with on-axis electrical dipole moments, where the dipole direction of each schematic molecule is indicated by its black-to-green shading, grouped into macroscopically nonpolar and polar types. The experiments reported here confirm the existence of the previously described paraelectric nematic (N) (3, 4), antiferroelectric smectic Z (SmZ_A) (16), and ferroelectric nematic (N_F) (4–7) phases, as well as the new SmA_F phase. These phases appear upon cooling in the general order indicated in the yellow-shaded area. Note that the N_F phase is missing in the 7N/DIO mixture, allowing for a direct smectic Z_A to smectic A_F transition. The solid, heavy lines depict smectic layering. The SmA_F phase is spontaneously ferroelectric, with polarization P~6 μC/cm² and polar order parameter P ~ 0.9, values comparable to those of the N_F phase of DIO (6) and RM734 (7). Polarization reversal is mediated by the motion of pure polarization reversal domain walls (heavy, dashed line). The antiferroelectric layer-by-layer alternation of polarization induces splay modulation of the director in the SmZ_A phase, but splay is suppressed in the ferroelectric N_F and SmA_F phases. (B) Structures and phase sequences of the liquid crystals and their mixtures studied here.

In contrast to the conventional dielectric SmA phase, the SmA_F phase exhibits a macroscopic polarization P, with the polarization in every layer pointing in the same direction, along the director, n, normal to the layer planes. The phase is uniaxial and has a high degree of polar order (polar order parameter P > 0.9). Domains of opposite polarization separated by polarization-reversal walls (sketched in Fig. 1A) are observed in regions with continuous smectic layering.

This ferroelectric phase is distinct from the phases previously described in several families of uniaxial "polar smectics", including the monolayer paraelectric SmA₁, the partial bilayer SmA_d, the antipolar bilayer SmA2 phase, and a variety of polarizationmodulated phases (SmA, SmC, SmC₂, etc.) of dipolar molecules (19-21), in that these all have zero net average polarization (22). Tournilhac and coworkers claimed initially to have observed macroscopic polarization normal to the layers in a small-molecule, SmA phase, based on evidence of piezoelectricity and nonlinear dielectric behavior (23, 24) but their subsequent X-ray scattering study revealed a smectic unit cell doubling (25), leading to the

conclusion that the phase in question was a bilayer smectic of the SmA_d variety and that the observed electrical effects were manifestations of bilayer antiferroelectricity. The SmA_F is also different from the orthogonal polar smectic phases exhibited by some bentcore mesogens, which form biaxial smectics with the spontaneous polarization oriented parallel to the smectic layers (26–28).

Results

X-Ray Scattering. We have previously carried out X-ray diffraction, polarized light microscopy, and polarization measurement studies of the single molecular components, DIO (9, 16) and 2N,7N (29), shown in Fig. 1B. Here, we focus on the binary mixtures 2N/DIO and 7N/DIO. All of our observations indicate that the N, N_F SmZ_A, and SmA_F phases observed in these different single components and/or in the mixtures exhibit common experimental characteristics and appear, respectively, to be the same phases in the different materials: the N phases are homogeneous, uniaxial nematics; the N_F phases are homogeneous, uniaxial nematics with a macroscopic polarization along the nematic director; and the SmZ_A is the same bilayer antiferroelectric phase in all of the components and mixtures, with a layer spacing $d_{\rm M} \sim 90 \text{Å}$ in DIO, $d_{\rm M} \sim 81 \text{Å}$ in the 2N/DIO mixture, and $d_{\rm M} \sim 60 \text{Å}$ in the 7N/DIO mixture. The period of the layer-by-layer antiferroelectric polarization alternation is $2d_{\rm M}$.

In this study, we describe the liquid crystal (LC) behavior of 50:50% 2N/DIO and 7N/DIO mixtures, both of which exhibit the SmA_F. We find that these mixtures show (i) similar scattering in the SmA_F phase from the SmA_F layering, with a fundamental SmA layer Bragg scattering peak at $q_{||} = (q_{||AF})n$, indicating layer spacing close to the mean molecular length; (ii) similar intense diffuse scattering in all of the phases (N, SmZ_A, N_F, and SmA_F) peaked at the SmA layer Bragg scattering peak position, indicating head-to-tail molecular positional correlations; (iii) no indication of a tendency for polar SmA antiferroectric bilayer ordering, i.e., no sharp or diffuse scattering feature at $q_{\parallel} = (1/2q_{\parallel AF})$; (iv) similar uniaxial birefringence; (v) similar SmA-like optical textures; (vi) similar response of the SmA_F to surface-alignment conditions and applied electric field; and (vii) similar polarization reversal dynamics in the SmZ_A phase and in the SmA_F phase. We discuss the two mixtures separately because of the differences in how the SmA_F grows in on cooling, 2N/DIO coming from the N_F phase, and 7N/DIO coming from the SmZ_A phase, as this condition strongly affects the textural morphology of the SmA_F as it grows

For the small-angle X-ray scattering (SAXS) and wide-angle X-ray scattering (WAXS) experiments, the mixtures were filled into 1-mm-diameter, thin-wall capillaries and the director n(yellow arrow in Fig. 2A) was aligned by an external magnetic field B (red arrow). The SAXS and WAXS were nonresonant, with diffraction images of the samples obtained in transmission on the Soft Matter Interfaces (SMI) beamline (12-ID) at National Synchrotron Light Source (NSLS) II, a microbeam with an energy of 16.1 keV and a beam size of 2 μ m × 25 μ m. The magnetic field produced general alignment in the capillary, but the SmZ_A and SmA_F textures were somewhat polydomain, with an ~10° mosaic distribution of azimuthal orientations of **n**. The z axis in the X-ray plots is taken to be along the director in the domain filling the illuminated volume.

2N/DIO. Typical SAXS and WAXS images obtained on cooling the 50:50% 2N/DIO mixture from the N_F to the SmA_F phase are shown in Fig. 2A. In the N_F phase at T = 57.9 °C, we observe a nematic-like, diffuse scattering arc peaked in azimuthal orientation with scattering vector \mathbf{q} along \mathbf{n} , coming from the head-totail pair correlation of the molecules along n. Line scans of the scattering intensity through these peaks are shown in Fig. 2B. As seen in the Inset of Fig. 2B, the SmAF phase is heralded by the appearance of a new, resolution-limited peak along $q_{||}$, first showing up at $T \sim 56\,^{\circ}\text{C}$, at $q_{\parallel \text{AF}} \sim 0.267\,\,\text{Å}^{-1}$, a wavevector very close to the diffuse nematic peak at $q_{\parallel} \sim 0.271\,\,\text{Å}^{-1}$. The Inset in Fig. 2A shows a single-domain Bragg spot on the $q_{\parallel AF} \sim$ 0.267 Å⁻¹ ring. This behavior indicates a first-order phase transition from the N_F to the SmA_F, in accord with our polarized light microscope observations. The corresponding layer spacing is $d_{AF} = 23.5$ Å, comparable to the concentration-weighted average molecular length of DIO (23.2 Å) and 2N (23.4 Å). The absence in the SAXS images of half-order peaks at $q_{\parallel} = q_{\parallel AF}/2$ indicates that there is no observed tendency for bilayer fluctuations or ordering in the SmA_F in this mixture. The WAXS diffraction image in Fig. 2A shows the second-harmonic scattering from the layers at $2q_{\parallel AF} \sim 0.53 \text{ Å}^{-1}$. The full width at half-maximum azimuthal mosaic distribution of n in the magnetically aligned sample is initially ~5°. The scattering pattern rotates in the SmA_F

phase on cooling due to dynamical textural rearrangements in the capillary (16), and at lower temperature, there is some detectable scattering from the layering at all azimuthal angles, as the magnetic torque is not strong enough to maintain the alignment of the increasingly rigid smectic layers.

7N/DIO. Typical SAXS diffraction images obtained on cooling the 50:50% 7N/DIO mixture from the SmZA to the SmAF phase are shown in Figs. 3A and 4. The SmA_F scattering is qualitatively similar to that of the 2N/DIO mixture. In the SmZ_A phase at T = 43.6 °C, the SAXS shows a diffuse, nematic-like scattering arc, peaked with scattering vector qalong n, coming from head-to-tail pair correlations of the molecules along $n \mid z$. Radial line scans of the scattering intensity along n (the white lines depicted in Fig. 3A) are shown in Fig. 3B.

As in the 2N/DIO mixture, the SmA_F phase is characterized by a new, resolution-limited peak along q_{\parallel} , first appearing at $T \sim$ 31 °C, at $q_{\parallel AF} \sim 0.245$ Å⁻¹, at the maximum of the diffuse nematic peak, as shown in the Inset of Fig. 3B. The corresponding layer spacing $d_{AF} = 25.6 \text{ Å}$ is comparable to the concentrationweighted average molecular length of DIO (23.2 Å) and 7N (29.1 Å). The absence in the SAXS images of half-order peaks at $q_{\parallel} = q_{\parallel AF}/2$ again indicates that there is no tendency to form bilayers. As in the 2N/DIO mixture, the scattering pattern rotates in the SmA_F phase due to dynamical textural rearrangements in the capillary with changing temperature (16). The scattering arc becomes wider in the SmA_F as the effectiveness of the magnetic field alignment is reduced on cooling.

Finally, the equatorial Bragg spots at $q_{\perp} = q_{\perp M}$ coming from the density modulation due to the smectic layering of the SmZ_A, which are observed in both the 2N/DIO and 7N/DIO mixtures, are shown in Fig. 4. These peaks are not visible in Figs. 2*A* or 3*A* because they are relatively weak.

Polarized optical transmission microscopy enables direct visualization of the director field, n(r), and, apart from its sign, of P(r). These observations provide key evidence for the macroscopic ferroelectric ordering, uniaxial optical textures, and fluid layer structure of the SmA_F phase of the 2N/DIO and 7N/DIO mixtures. In these cells, z is the alignment layer buffing direction, x is the coordinate normal to the plates, and the director field n(r) is parallel to the plates but may or may not be along the buffing.

7N/DIO. The 50:50% 7N/DIO mixture was studied in a d =3.5 µm cell with antiparallel surface rubbing (an antipolar cell) with two indium tin oxide (ITO) electrodes on one surface for applying an in-plane field across a 1-mm gap. In the N phase, the LC formed a uniformly aligned monodomain with n along the buffing direction, as previously observed in the nematic phase of DIO (16). In the 7N/DIO mixture with no field applied, there is little change in sample appearance with temperature, the nematic texture being maintained upon cooling into the SmZ_A and SmA_F phases, as seen in Fig. 3 C, 1 and 2. At the SmZ_A to SmA_F transition, the SmZ_A layers parallel to ndisappear while new SmA_F layers, normal to **n**, form. The birefringence color is a uniform blue-green everywhere in the cell and changes only slightly during the N \rightarrow SmZ_A \rightarrow SmA_F cooling sequence, providing evidence that the phase is uniaxial or only weakly biaxial and that the optical anisotropy is nearly the same in all three phases. The uniaxiality of the N phase and the weak biaxiality of the SmZ_A have been demonstrated previously (16).

The SmZ_A layers adopt bookshelf geometry, with the smectic layers normal to the plates and with Rapini-Papoular type anchoring of the molecules, aligning n along the buffing direction z and the SmZ_A layer normal along y. Buffed layers for

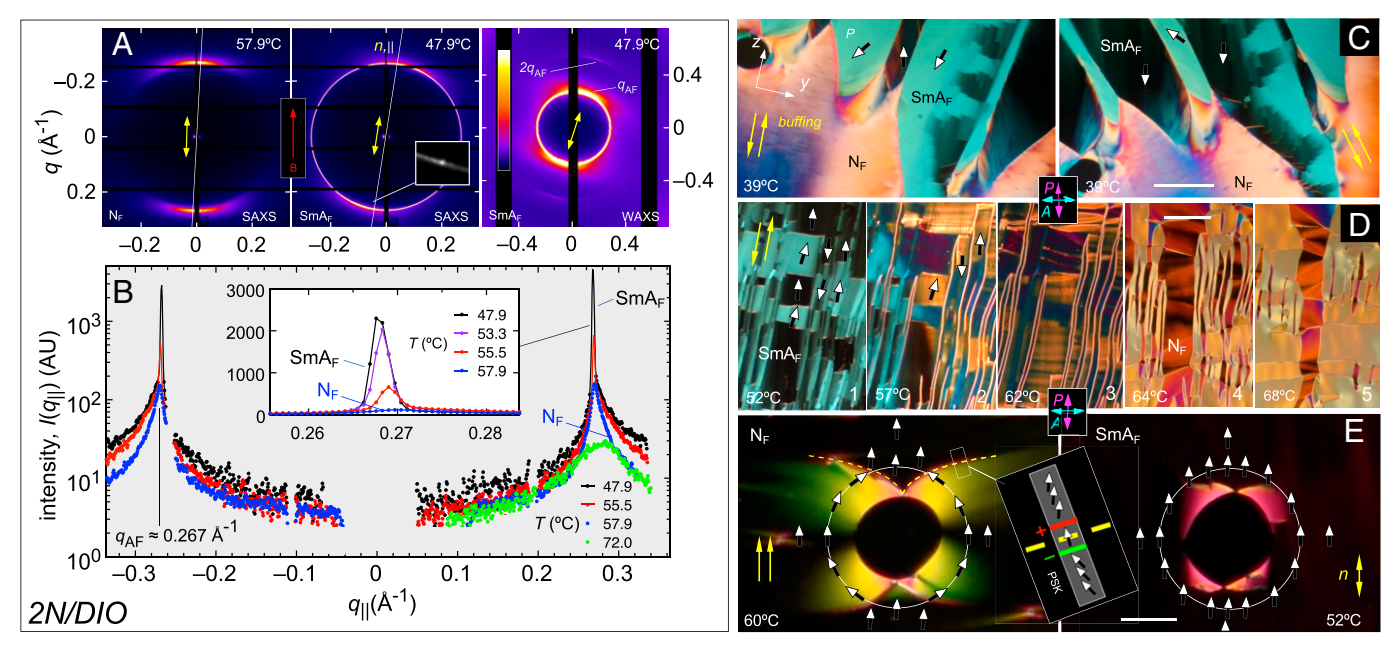


Fig. 2. X-ray scattering and polarized microscopy textures of the N_F and SmA_F phases in the 50:50% 2N/DIO mixture. (A and B) Typical nonresonant SAXS and WAXS obtained on cooling from N_F to SmA_F. In the N_F phase at 57.9 °C, there are nematic-like diffuse scattering arcs, peaked along $\bf n$ at $q_{\parallel} \sim 0.27~{\rm \AA}^{-1}$ coming from head-to-tail correlation of the mixture molecules. B shows radial intensity scans along the n, q_{\parallel} direction (the white lines in A) at different temperatures. In this experiment, the scattering pattern rotates azimuthally by as much as 10° due to textural reorganization within the capillary as the smectic layers form. The initial high-T correlation peak sharpens significantly but remains diffuse on cooling (green curve \rightarrow blue curve), until distinct, resolutionlimited SmA_F Bragg reflections appear in the n direction at $T \sim 56$ °C, as shown by the red curve in B and the Inset in A, indicative of smectic ordering with the layer planes normal to n. The Inset in A shows a single-domain Bragg spot on the $q_{\parallel AF} \sim 0.267$ Å $^{-1}$ ring. This scattering vector corresponds to a SmA_F layer spacing of 23.5 Å, close to the wt% average molecular length of DIO (23.2 Å) and 2N (23.4 Å). The polarized light microscope images in C and D show the 50:50 wt% 2N/DIO mixture in a d = 3.5- μ m-thick, antipolar cell (with antiparallel surface rubbing) and in E a d = 3.5- μ m-thick, synpolar cell (with parallel surface rubbing) face rubbing), both in the absence of applied field. (C) The SmA_F phase grows in, upon slow cooling, from the top of this region of the cell at $T \sim 55$ °C, as irregular, polygonal domains of layers with n and P oriented parallel to the cell plates and uniformly aligned throughout their volume. The existing N_F material is in a surface-induced, π-twisted state, with P along the (antiparallel) buffing at the surfaces. This twisted state imposes no preferred bulk orientation of the polarization. As a result, the advancing SmA_F domains are ambivalent in their choice of polarization alignment and appear with P aligned in various directions as shown. (D) A different part of the cell, now observed on heating from the SmA_F to the N_F phase. At low temperature, shown in 1, these SmA_F domains have n generally along the buffing and are extended locally along n to minimize polarization space charge, with the domains separated by smallangle melted grain boundaries and polarization-stabilized kinks (PSKs), sketched in the Inset in E, which mediate small changes in the orientation of P versus position, z. In contrast, finite $(\partial P_z/\partial y)$ does not generate polarization charge, enabling domains of opposite sign of **P** along x to be neighbors along y, in the absence of space charge. Upon heating to the N_F, the boundaries between these adjacent domains transform into splay-bend walls (bright lines in 2 and 3), which then broaden into π-twist domains that eventually cover most of the cell (4 and 5). (E) In a synpolar cell, a uniform monodomain is formed on cooling, with n in both the N_F and SmA_F phases aligned along the buffing direction, giving excellent extinction, and P along the polar orientation preferred by the unidirectional buffing in the N_F phase. The images show the deformation of this otherwise uniform texture enforced by an air bubble extending through the thickness of the cell (see text). Scale bars: (C) 500 μ m, (D) 200 μ m, and (E) 100 μ m.

azimuthal planar alignment appear to operate in a fashion similar to that of nematics, with the exception that unidirectional buffing induces polar orientation of P (10, 30). The transition of the SmZ_A , with its layer-by-layer alternation of P, to the SmA_F phase is achieved by a coarsening process in which layers with the same sign of P coalesce into broader stripes of uniform polarization extended along z, leading to a texture of irregular, needle-like ferroelectric domains of alternating polarization in the SmA_F . This process takes place with n remaining along the buffing direction, producing only subtle changes in the textures in the absence of applied field (compare Fig. 3 C, 1 and 2), with n, z, and P all colinear. However, it can be visualized by application of an in-plane electric field normal to n. This induces rotation of P in opposite directions in domains with opposite polarization, facilitating and inducing the coarsening of the domain pattern (Fig. 3 C, 3-6). This electric field response becomes increasingly dramatic as the stripes coarsen from the nanoscale to the microscale.

After extended application of weak electric fields, the SmA_F cell anneals, in the absence of further applied field, into long, rectangular bookshelf domains with uniform birefringence and excellent extinction typical of weakly oriented SmA textures, as shown in Fig. 3 *D*, *I* and *2*. Sufficiently large transverse direct current fields can completely reorient the SmA_F layers so that

P and n become aligned along E, normal to the buffing direction (Fig. 3 D, 5). In the N_F phase, this kind of global, fieldinduced reorientation is essentially thresholdless, with the polarization reversing readily on applied field reversal, but in the SmA_F phase, there is a distinct threshold for switching and hysteresis in the response, manifest in the polarization data of SI Appendix, Fig. S1. This behavior can be understood by considering that field-induced reorientation of a spatially uniform SmA_F can only be accommodated by the generation of a population of gliding edge-dislocations, an inherently nonlinear process. The effect of this threshold is immediately apparent in the electro-optic behavior in cells with in-plane electrodes. In an applied field, these domains reorient, buckle, and, in sufficiently large applied field, coarsen to form large domains with the n and P both oriented along the field, normal to the buffing direction z (D3 to 5). Thus, it appears that, during fieldinduced reorientation, n and P remain coupled together, with the threshold originating from the elasticity and plasticity of the smectic layering. This threshold also results in the appearance of a coercive field in the polarization hysteresis (SI Appendix, Fig. S1). The N_F phase typically responds readily to in-plane applied electric fields present anywhere in the cell, including above metal or ITO electrodes, and even to small (V/cm) fringing fields far from any electrodes. In the SmA_F

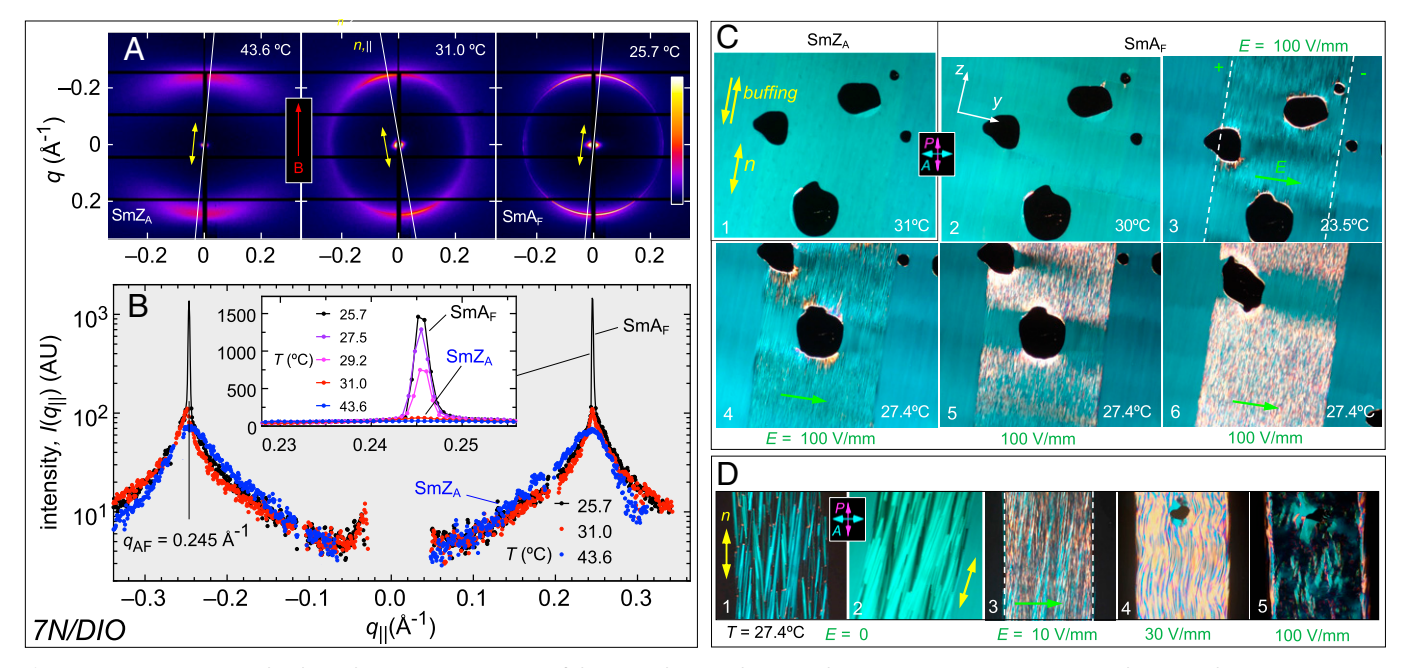


Fig. 3. X-ray scattering and polarized microscopy textures of the N_F and SmA_F phases in the 50:50% 7N/DIO mixture. (A and B) Typical nonresonant SAXS obtained on cooling from SmZ_A to SmA_F. In the SmZ_A phase at 43.6 °C, the SAXS shows a diffuse scattering arc, peaked along n at $q_{\parallel} \sim 0.27 \text{ Å}^{-1}$, arising from head-to-tail correlation of the mixture molecules, a feature also observed in the diffraction patterns of DIO (16). (B) Radial intensity scans along the n, q 1 direction (the white lines in A) at different temperatures. As in the 2N mixture, the scattering pattern rotates and spreads due to textural reorganization within the capillary as the SmZ_A layers are replaced by SmA_F layers. The scattering from the SmZ_A layering is not visible here but is shown in Fig. 4. Upon cooling, the diffuse peaks sharpen somewhat (much less than in the 2N mixture), the SmZ_A layering peaks along \mathbf{q}_{\perp} weaken and disappear, and at $T \sim 31$ °C, distinct, resolution-limited Bragg reflections appear along q_{\parallel} as shown in the *Inset*, indicative of smectic ordering with the layer planes normal to n. The scattering wavevector, $q_{\parallel AF} \sim 0.245 \text{ Å}^{-1}$, corresponds to a SnA_F layer spacing of 25.6 Å, close to the wt% average molecular length of DIO (23.2 Å) and 7N (29.1 Å). The position of the SmA_F scattering peak is very close to that of the diffuse nematic peak, as expected for an orthogonal smectic phase. (C and D) Polarized microscopy images of an antipolar cell with a $d = 3.5 \mu m$ spacing and electrodes spaced by 1 mm (dashed white lines) for applying an in-plane field normal to the buffing direction z. In the absence of applied field, the SmZ_A texture shows nearly perfect planar alignment with n parallel to z, from which state there are only subtle changes upon transitioning to the SmA_F (1 and 2). This is because, while the antiparallel buffing orients the director, it does not favor either of the antiferroelectric polarization directions. As a result, at the transition, the nanoscale antiferroelectric SmZ_A layers normal to y simply coarsen into SmA_F domains extended along n, normal to the newly forming SmA_F layers and alternating in polarization along y. The director remains uniform through this change, and the two phases are consequently very similar in appearance. However, applying a probe E field (\sim 100 V/mm) along y (3), causes director reorientation within fixed stripes, wherein the directors in stripes of opposite Pz rotate away from extinction in opposite directions, giving optical contrasting stripes of opposite polarity extended along z. 4-6 shows a time sequence of these domains coarsening in an E = 100 V/mm field. The circular black regions are air bubbles, which have much higher electrical impedance than the adjacent liquid crystal, leaving its texture undisturbed. (D) Annealing after such field treatment yields an inhomogeneous smectic fan texture (1 and 2). In an applied field, these domains reorient, buckle, and, in sufficiently large fields, coarsen to form large domains with n and P both oriented along the field, normal to the buffing direction (3-5). Scale: the electrode gap (dashed white lines in C and D) is 1 mm wide.

phase, in contrast, this response becomes subthreshold and is eliminated from these peripheral areas, with electro-optic effects confined to the designated active areas of the cell between the electrodes, where the field is strongest, as seen in Fig. 3 D, 3-5. The field on the LC is reduced adjacent to bubbles in the electrode gap in Fig. 3 C, 3-6, due to their higher electrical impedance.

2N/DIO. The 50:50% 2N/DIO mixture was studied in an antipolar $d = 3.5 \mu m$ cell (with antiparallel surface rubbing) and in a synpolar $d = 5 \mu m$ cell (with parallel surface buffing). In the antipolar cell, the surface anchoring imposes a twist structure in the N_F phase in which the director/polarization field n(r), P(r) rotates by π through the thickness of the cell (11). The twisted N_F state appears from pinkish to blueish in Fig. 2C, which shows the cell being cooled through the first-order N_F to SmA_F transition, with blue-green SmA_F domains growing in the upper part of the field of view. The observation that the SmA_F domains can be rotated to extinction between crossed polarizers indicates that the director twist has been expelled such that, at a point in the SmA_F area, the director n(y,z) has a local in-plane (y,z) orientation that is the same for all x. The uniformity of the birefringence color indicates that the phase has a principal optic axis parallel to the plates and that the phase is uniaxial, not biaxial. The growing SmA_F domains are

not strongly orientationally aligned by the cell surfaces initially, most likely because of the ambivalence of these now polar domains toward the antipolar surfaces. The results of application of a weak probe electric field normal to the director are shown in Fig. 5 A-C, confirming that each domain is internally homogeneously polar (black/white arrows) with orientation along the local director, some pointing up and some pointing down. The expulsion of bend and twist of n(r) by the SmA_F layering, and expulsion of splay of n(r) in order to eliminate polarization charge, results in steady-state textures of uniformly oriented SmA_F blocks, as shown in Fig. 2D, in which there are distinct domain boundaries running either parallel or perpendicular to n. The boundaries parallel to n (approximately vertical in these images) are polarization-reversal walls like those found in the N_F phase (7), while those perpendicular to n are either melted grain boundaries of the type commonly found in SmA phases not completely aligned by weak buffing (31) or are polarization-stabilized kinks (PSKs) (32), as sketched in the *Inset* of Fig. 2E. Changes in the sign of P(r) across the horizontal boundaries would generate maximal space charge and are thus avoided, with jumps in the orientation of P(r) at these locations being limited to 10° or less. In general, there is a tendency to form long SmA_F domains of uniform polarization extended along the director, as seen in Figs. 2D and 3D. The

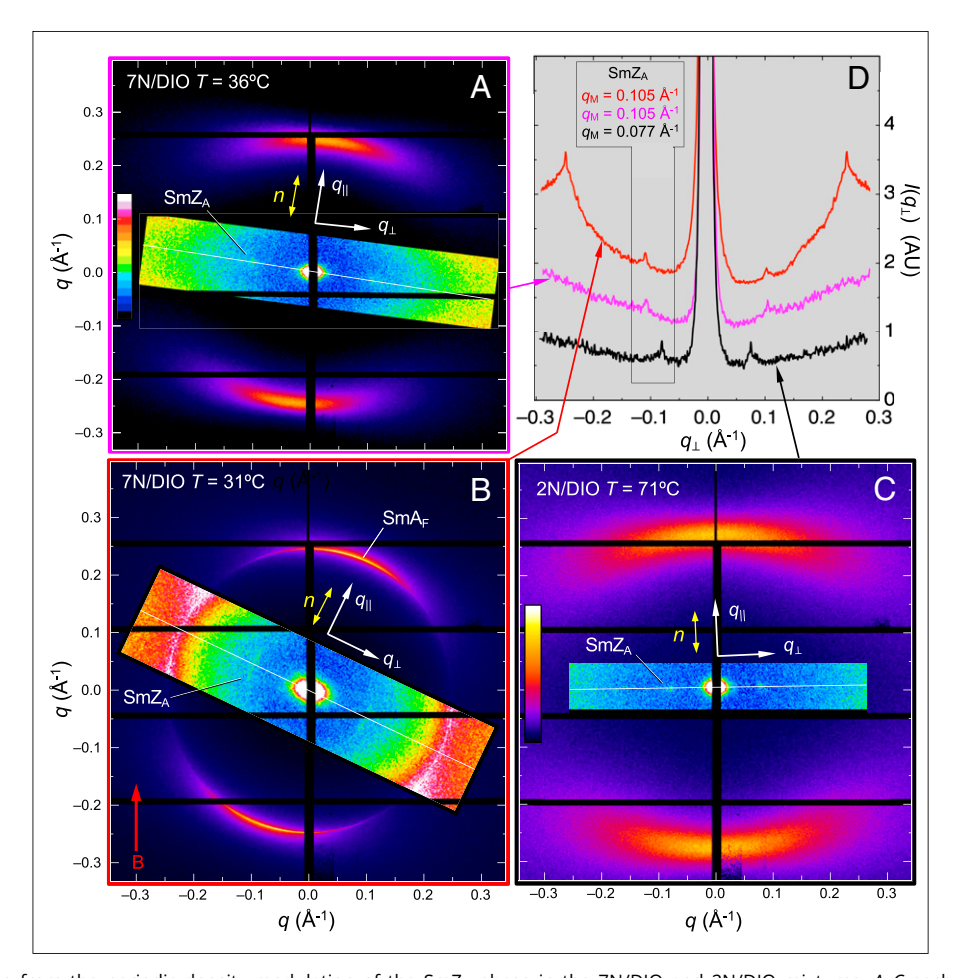


Fig. 4. X-ray diffraction from the periodic density modulation of the SmZ_A phase in the 7N/DIO and 2N/DIO mixtures. A-C each show a complete SAXS image of the scattered intensity, I(q), using the color gamut shown in C. The rectangular overlays show I(q) after histogram stretching and using the color gamut in A, revealing the weak scattering peaks from the SmZ_A layer modulation along q_{\perp} . The director is aligned in the nematic phase by a magnetic field, B, but rearrangements of the sample in the capillary during cooling lead to some inhomogeneity of the SmZ_A and SmA_F layer orientation. (A) At T = 36°C, the 7N/DIO mixture is in the SmZ_A phase, as evidenced by the scattering along q_{\perp} . The diffuse peaks along $q_{||}$, parallel to the director, come from short-ranged, end-to-end molecular correlations. The SmZ_A peak locations, at $|q_{\perp}| = q_{\rm M} \sim 0.105~{\rm \AA}^{-1}$, correspond to a layer spacing of $d_{\rm M} \sim 60~{\rm \AA}$, essentially independent of $T_{\perp}(0)$ Cooling to $T_{\perp}(0)$ Co pendent of T. (B) Cooling to T = 31 °C initiates a weakly first-order phase transition to the SmA_F, with sharp scattering appearing simultaneously from both the SmZ_A and SmA_F layers. The SmZ_A peaks at this temperature appear as extended arcs. The SmZ_A scattering disappears ~0.5 °C below the onset of the SmZ_A-SmA_F transition, i.e., there is a narrow range of T where both the SmZ_A and SmA_F peaks are present, which we attribute to two-phase coexistence at a first-order transition. (C) Diffraction from the 2N/DIO mixture at T = 71 °C, in the middle of the SmZ_A phase region. (D) Radial scans of the scattered intensity along q_{\perp} , normal to the director, obtained by azimuthally averaging I(q) over the range of q that includes the SmZ_A peaks. The low-temperature scan of B exhibits, in addition to the SmZ_A peaks, scattering at $q_{\perp} = 0.245 \text{ Å}^{-1}$ from a few SmA_F domains. While dwarfing the SmZ_A peaks, this latter intensity is orders of magnitude smaller than the main SmA_F scattering along $q_{||}$.

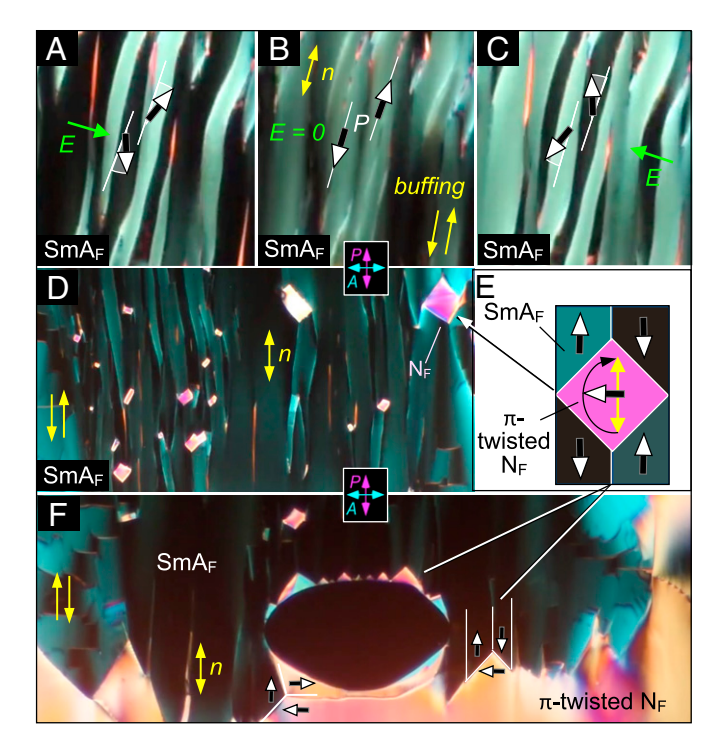
internal variation of orientation within the blocks is generally only a few degrees and tends to be bend of the director field, which must be mediated by edge-dislocations in the SmA_F layering system.

More detailed structures of the transition regime that mediates the growth of the uniform SmA_F domains into the twisted region are shown in Fig. 5 D-F. Here, remnant diamond-shaped N_F twist domains connect to surrounding uniform SmA_F domains by forming PSK domain boundaries with the polarization directions in the sample midplane indicated in Fig. 5E. Similar structures constitute the zigzag SmA_F–N_F boundary lines in Fig. 5F.

If the SmA_F is heated into the N_F phase, the removal of the layering constraints enables the polarization-reversal walls to restructure into nematic splay-bend walls (7) extended along the director, separated by areas of uniform polarization, as seen in Fig. 2 D, 2 and 3. The horizontal melted grain boundaries disappear in the absence of layering, while the horizontal PSK lines can persist into the N_F but then also melt away, leaving only the splay-bend walls (bright lines in Fig. 2 D, 2 and 3). Because of the antiparallel boundary conditions, the initially

uniform N_F states are only metastable and the inherently twisted cores of the splay-bend walls act as nucleation sites for the formation of lower-energy, twisted domains, which eventually spread to cover the entire area (Fig. 2 D, 5).

In the synpolar cell, the surface treatment stabilizes monodomains in which n is homogeneously aligned along the buffing direction. The texture and birefringence of these monodomains barely change on cooling through the N-SmZ_A-N_F-SmA_F phases, exhibiting excellent extinction between crossed polarizers in the N_F and SmA_F phases except near air bubbles, as seen in Fig. 2E. The first image shows how the uniform background N_F director field favored by the cell surfaces is distorted to accommodate the nonuniform n(r) orientation imposed by the boundary conditions at the edges of the bubble, where the n(r) field is tangential, a configuration that requires only bend of the director and minimizes the amount of space-charge deposited at the LC/air interface. On the sides of the bubble, the director field distortion relaxes continuously with distance, with the director field eventually becoming indistinguishable from the surrounding uniform state. At the top and bottom of



 $\textbf{Fig. 5.} \quad \text{Response of } \text{SmA}_{\text{F}} \text{ texture to applied field. The cell is the same as in}$ Fig. 2 C and D ($d=3.5~\mu m$ cell with antiparallel surface rubbing), with SmA_F domains (green) that have replaced a π -twisted N_F phase (yellow/pink). The twisted N_F does not bias the polarization preference, so domains of both orientations of P should spontaneously appear in the SmA_F. (A-C) This can be tested by applying an in-plane electric field \boldsymbol{E} that is transverse (substantially normal to \mathbf{n} and \mathbf{P}). The opposite induced rotations in A and C confirm that there is a macroscopic, uniform polarization within each domain and that its direction along n alternates from domain to domain. (D-F) Diamond-shaped inclusions of twisted N_F mediate the reversal (D) or termination (E, F) of up-down pairs of SmA_F domains. The white domain boundaries in E are PSKs (32), localized reorientations of P stabilized by the attraction of sheets of polarization charge of opposite sign, as shown in Fig. 2E.

the bubble, however, the 90° angular mismatch of the circumferential P(r) and the uniform background is accommodated by a "fracture" of P(r) in the form of a PSK (32), sketched in the Inset. The PSK has a minimum-energy discontinuity in P(r), with an internal structure determined by the balance of Frank elastic and electrostatic interactions, the latter manifested as an attraction between sheets of polarization charge of opposite sign (red and green in the Inset), which stabilizes the wall. The kink orientation locally bisects the angle between the incoming and outgoing P(r) directions, leading to a globally parabolic boundary between the regions with uniform and circular bent-director fields having minimal bulk polarization charge. Such two-dimensional parabolic textures, induced by the suppression of director splay, are the structural analogs of parabolic focal conics in smectics, which are induced by the suppression of director bend (33). These parabolic defects are readily observed in N_F cells, where P(r) is parallel to the bounding plates, its typically preferred orientation.

At the N_F-SmA_F transition, the areas of uniform director orientation expand, a result of the appearance of the SmA-like layering. In the absence of edge and screw dislocations, smectics expel both bend and twist of n(r), allowing, in inhomogeneously aligned nonpolar SmA, layering defects only in the form of focal conic domains, as these require only splay of n(r). However, in the polar SmA_F phase, splay is also suppressed because of the associated polarization charge, leading to a strong tendency to form domains of uniform n(r). As the smectic layers form on cooling, the bent-director region near the bubble, in which there is both bend and twist of n(r), is therefore reduced in size, as shown in the second image of Fig. 2E. In the remaining region near the bubble, where there is bend and twist of the director, the induced splay and twist of the smectic layering is accommodated by layer edge and screw dislocations, neither of which generates polarization space charge.

The observed transitions to the SmA_F phase, whether N_F to SmA_F or SmZ_A to SmA_F, are first order but maintain uniform planar director orientation in cells having parallel polar anchoring (parallel, unidirectional surface buffing). The SmZ_A to SmA_F transition in such cells is particularly subtle, with little change observed in birefringence or texture through the transition.

Polarization Dynamics and Field-Induced Phase Transitions. The polarization was measured in $d = 17 \mu m$, bare-ITO sandwich cells with planar alignment of n and bookshelf layering of the smectics at zero field, using low-frequency (8 Hz) triangle

waves. The electrical response of the 2N/DIO and 7N/DIO mixtures as a function of temperature is summarized in SI Appendix, Fig. S1. At the beginning of the current-voltage cycle, shown in SI Appendix, Fig. S1A for the 2N mixture, the applied voltage is large and negative ($V(t) \sim -30 \text{ V}$), at which time any ions have been pulled to the cell surfaces so there is no ion current. In the N phase (T > 84 °C), the current shows a bump following the sign change of V(t), which we attribute to ions. In the SmZ_A phase (84 °C > T > 68 °C), the polarization current is combined with the ion current following each sign change of V(t), so the polarization P(T) is obtained by doubling the I(t) area left of the center line, where the ion current, taken as that at the lowest temperature in the N phase, is small and subtracted out. The SmZ_A exhibits LC repolarization peaks that appear when the applied negative voltage is decreasing, growing in area and with their peak center voltages $V_{\rm FA}$ moving toward zero on cooling, behavior very similar to that of neat DIO (see Fig. 5 in ref. (7)). This is typical antiferroelectric behavior, the peaks marking the return at finite voltage of the field-induced ferroelectric state to the antiferroelectric ground state. In the N_F phase, the Goldstone-mode mediated reorientation and reversal of P produces a current peak at the zero crossing of V(t) (cyan scans), followed by an ion peak at some later time. P(T), taken as the area of the big peak, is found to grow more slowly on cooling in the N_F than that of neat DIO or RM734 (7) or their mixtures (9), possibly a result of the increasing short-range SmA_F order. At the transition to the SmA_F phase, P jumps up to a T-independent value and the ion current disappears altogether due to screening of the field in the LC due to polarization charge. Polarization reversal occurs after the zero crossing, at a finite voltage corresponding to the coercive field E_c plotted as solid symbols in SI Appendix, Fig. S1B and shown schematically in the adjoining hysteresis loop. SI Appendix, Fig. S1 C and D show the results for the 7N/DIO mixture, where the Goldstone feature of the N_F is absent, heralding the direct SmZ_A to SmA_F transition. The N phase again exhibits a large current peak following the sign change of V(t), so P(T) in the SmZ_A is again obtained by doubling the I(t) area left of the center line, with the N phase current as a background. As in SI Appendix, Fig. S1 A and B, the ion current disappears in the SmA_F phase and the integration is carried out

Discussion

over the whole V(t) range (Fig. 6).

These observations, and the recent report that replacing only a single H atom on DIO with an F atom can produce a homolog that exhibits the SmA_F phase as a single molecular component

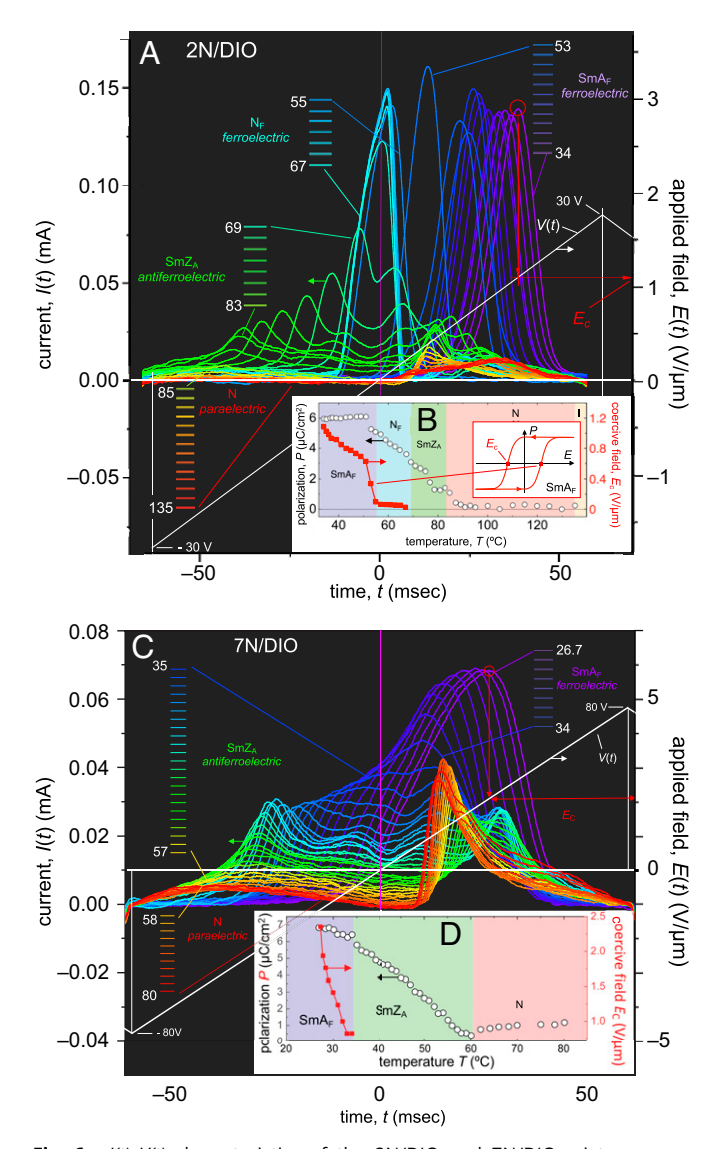


Fig. 6. I(t)-V(t) characteristics of the 2N/DIO and 7N/DIO mixtures as a function of temperature with 8 Hz triangle-wave voltage (white trace) applied to a $d=17~\mu m$ bare ITO-sandwich cell with bookshelf layering in the smectic phases. (A) 2N/DIO current response - The plots show the current response during an N \rightarrow SmZ_A \rightarrow N_F \rightarrow SmA_F cooling run. In the N phase (T > 84 °C), the current shows only an ion peak (red to orange curves) following the sign change of V(t). In the SmZ_A phase (84 °C > T > 68 °C, green curves), two polarization peaks are seen during this half-cycle of the applied voltage, growing in area and occurring at smaller voltage on cooling. This is typical antiferroelectric behavior, the peaks marking the transition at finite voltage between the field-induced ferroelectric states and the equilibrium antiferroelectric state. In the N_F phase, (cyan curves) the Goldstone-mode mediated reorientation appears "thresholdless" and reversal of P produces a current peak at the zero-crossing of V(t). Unlike pure DIO, where the saturation P is achieved at high T in the $N_{\rm F}$ phase, in the 2N/DIO mixture it increases linearly to near the saturation value, and then saturates in the SmA_F phase. In the SmA_F phase (blue to purple curves), the ion current disappears and polarization reversal peak occurs at positive voltage corresponding to the coercive field E_c , shown, by way of example, for T = 34 °C (red construction). (B) 2N/DIO polarization – Polarization values P(T) [open circles] were obtained by integrating the current. In the SmZ_A phase, the polarization current generated following each zerocrossing of V(t) interacts in a complex way with the ion current, so P(T) is obtained in this case by doubling the area of the current peak generated for V(t) < 0. The coercive field, E_{cr} is also shown as a function of T [solid symbols]. Note that in the N_F and SmA_F the ion peak is not observed because ionic charge is completely screened by the polarization charge. (C) 7N/DIO current response - The plots show the current response during an N \rightarrow SmZ_A \rightarrow SmA_F cooling run, exhibiting the same overall features as the 2N/DIO mixture, except for the notable absence of the current peak at the zero-crossing of V(t), indicative of an N_F phase. The 7N mixture gives the largest ion currents among the mixtures and DIO, but in the 7N nematic this may be some kind of antiferroelectric pretransitional effect of

(34), adds an exciting new dimension to the N_F realm. The N_F, chiral N_F, and SmZ_A discoveries have each opened unanticipated doors to soft matter science and broadened the potential for technology, and here, the SmA_F joins in this development. The SmA_F is a spontaneously polar, layered fluid, the long-soughtafter proper SmA_F liquid. While its reorientable macroscopic spontaneous polarization is now definitively proven, understanding its nanoscale origin is another matter entirely, a problem which must be considered in the context of molecules such as RM734 and DIO, which are spontaneously and strongly polar, even though their structure differs very little from those of innumerable N mesogens, which form only nonpolar phases.

RM734 and DIO share the common feature of developing near-perfect spontaneous ferroelectric polar ordering over almost the entire N_F phase temperature range, achieving the polar order parameter value of P = $\langle \cos \theta \rangle \sim 0.9$ (7, 9), where θ is the angle between a given molecular dipole and the local P. Atomistic simulations show this saturation polarization value, $P \sim 6 \,\mu\text{C/cm}^2$, to be determined by orientation fluctuations of a state with almost perfect binary order (all positive molecular ends directed along **P**), as discussed in SI Appendix, section S3. In contrast, the 2N/DIO and 7N/DIO mixtures achieve such saturated polar ordering only in the SmA_F phase, in discontinuous jumps from less-well-ordered N_F and SmZ_A phases, respectively.

Atomistic simulations of RM734 also show that a factor contributing to this large saturation value of the polar order parameter is head-to-tail polar electrostatic association of the rod-shaped mesogens (7). This association produces diffuse peaks in the paircorrelation function of molecular position along the director, n, at a separation within an angstrom or so of the molecular length, l, and a corresponding diffuse peak in the X-ray structure factor at $|q_{||}| = q_{||AF} \sim 2\pi/l \sim 0.25 \text{ Å}^{-1}$. This peak appears in RM734 and DIO (SI Appendix, Figs. S2-S4 (9)), and in the 2N/DIO and 7N/DIO mixtures (Figs. 2-4). Its line shape can be used to estimate molecular positional correlation lengths, $\xi_{||}(T)$ and $\xi_{\perp}(T)$ (SI Appendix, Sec. S3). In the mixtures, at temperatures well above the transition to the SmA_F phase (Figs. 3B and 4C), we find $\xi_{||} \sim$ 30 Å and $\xi_{\perp} \sim 4$ Å, indicating linear, end-to-end, chain-like associations of approximately two to three molecules, without much side-by-side interaction, and only a weak temperature dependence. In the RM734/DIO mixtures, the saturation P is achieved in the N_F under this circumstance. In the 2N and 7N mixtures, however, the corresponding polarization values are well below saturation but grow continuously with decreasing T, as shown in SIAppendix, Fig. S1. Additionally, as the mixtures are cooled into the range ~10 °C above the SmA_F transition, the diffuse scattering peak substantially narrows in q and the correlation lengths exhibit a second-order type, pretransitional divergence, increasing in 2N/DIO to $\xi_{||} \sim 200$ Å and $\xi_{\perp} \sim 14$ Å at T = 55 °C, where the first-order transition to the SmA_F takes place for this mixture. At this transition, the polarization jumps to saturation and Bragg peaks appear at $|q_{\parallel}| = q_{\parallel AF}$, at the spacing of the diffuse peak in the X-ray structure factor, and with a resolution-limited width $(\xi_{\parallel}, \xi_{\perp} \sim 700 \text{ Å})$. This indicates that head-to-tail molecular association, which grows with increasing P in the N_F and SmZ_A phases, is cooperatively coupled to, and mutually promotes, the SmA layering.

the nematic, since the current peak observed at positive voltage evolves into the SmZ_A polarization peak with decreasing T. As with the 2N/DIO mixture the ion peak is not observed in the ferroelectric phase. (D) 7N/DIO polarization - Polarization values P(T) [open circles] were obtained by integrating the current as before, increasing substantially and monotonically in the SmZ_A and saturating in the SmA_F.

These X-ray features, the observed P(T) values, and the atomistic simulations of RM734 indicate that the appearance of the SmA_F phase is a cooperative coupling of dynamic headto-tail, polar, chain-like correlations with SmA layering correlations. This sort of ordering may be compared with that of the antiferroelectric uniaxial polar smectics of rod-shaped molecules noted above (19-21), in which the end-to-end association preference is antiferroelectric (with head-to-head/tail-to-tail chain correlations) rather than ferroelectric. When this kind of association is dominant, the resulting phases are antiferroelectric and a rich palette of nematic, smectic, and re-entrant phases emerges, controlled by the preferred relative positions of neighboring chains along the director. For example, side-by-side association of ends irrespective of whether they are heads or tails results in the monolayer SmA₁ phase, a nonpolar dielectric with a layer spacing close to the molecular length; condensation of paired heads in planes gives the antiferroelectric bilayer ordering of the SmA2 phase; and alternation of domains of paired heads and tails in a plane gives the modulated SmA phase. Nematic phases appear as a result of frustration between competing smectics of different layer periodicity.

It appears that, with the coming of the SmZ_A and SmA_F phases, a similar story may be emerging in the N_F realm, this one based on polar head-to-tail correlations. The SmA_F is apparently a monolayer smectic, a ferroelectric SmA1 in the terminology of the earlier polar smectic literature, with some degree of side-by-side ordering of chains having parallel polarizations. In this regard, it is worth recalling that the antiferroelectric polar smectic phases and the transitions between them have been modeled with some success by Berker and coworkers, who formulated hexagonal lattice (frustrated spin-gas) models, comprising finite-length columns of molecules with intracolumn, end-to-end interactions and intercolumn, side-by-side interactions (35-38). The simplest useful versions of these models are lattices of three distinct, finite-length column configurations, which capture the inherent frustration of hexagonally packing antiferroelectric columns interacting side by side. Such models enable exact statistical mechanics to be carried out, revealing theoretically the rich polymorphism of the antiferroelectric smectic polar phases and describing well multiply re-entrant phase sequences, including the N, SmA_d, reentrant N, and SmA₁ phases. While the focus of this earlier work has been on antiferroelectricity, this approach has recently been applied by Madhusudhana (39) to N_F ordering, showing that macroscopic ferroelectricity is achievable with model dipolar rods with similar dimensions and molecular-charge distribution to the molecules of the N_F realm. The application of such models to the SmA_F phase should be particularly revealing since, being a monolayer SmA1, the SmAF seems to require the ferroelectric ordering of side-by-side molecules. An effective approach to pursuing such modeling will be to use atomistic simulation to evaluate the actual forces between side-by-side chains.

Materials and Methods

The mixtures were studied using standard LC phase analysis techniques described previously (7, 10, 16), including polarized transmission optical microscopy observation of LC textures and their response to electric field, X-ray scattering (SAXS and WAXS), and techniques for measuring polarization and determining electro-optic response.

- P. Debye, Einige Resultate einer kinetischen Theorie der Isolatoren. Phys. Z. 13, 97-100
- M. Born, Über anisotrope Flüssigkeiten. Versuch einer Theorie der flüssigen Kristalle und des elektrischen Kerr-Effekts in Flüssigkeiten. Sitzungsber. Preuss. Akad Wiss. 30, 614-650 (1916).
- R. J. Mandle, S. J. Cowling, J. W. Goodby, A nematic to nematic transformation exhibited by a rod-like liquid crystal. Phys. Chem. Chem. Phys. 19, 11429-11435 (2017).
- A. Mertelj et al., Splay nematic phase. Phys. Rev. X 8, 041025 (2018).

Materials. DIO, shown in Fig. 1 and first reported in ref. (6), was synthesized for these experiments as described in ref. (9). Synthesis of AUUQU2N and AUU-QU7N, also shown in Fig. 1, followed that of AUUQU3N, described in ref. (40). The phase transition temperatures obtained upon slow cooling (~1 °C/min) are shown in Fig. 1. Optical microscopy as in Figs. 2 and 3, polarization measurements as in SI Appendix, Fig. S1, and changes in the X-ray scattering peak intensity as in Figs. 2A and 3A were used to locate the transitions. The 2N/DIO and 7N/DIO mixtures can be cooled at -1 °C/min to 25 °C, where they exhibit the SmA_F phase, which is monotropic with respect to crystallization. Crystallization proceeds very slowly, however, with samples remaining for days to weeks in the SmA_F phase. Upon heating, the fully crystalized 2N/DIO and 7N/DIO mixtures melt over a few °C range, at around 85 °C, into the N phase.

X-Ray Scattering. For the SAXS and WAXS experiments, the LC samples were filled into 1-mm-diameter, thin-wall capillaries. The director \boldsymbol{n} was aligned with an external magnetic field normal to the beam. Diffraction data presented here were obtained on the SMI beamline at NSLS II with a photon energy of 16 keV (wavelength = 0.775 Å). At this wavelength, the desired range of scattering vectors ($q < 0.5 \text{ Å}^{-1}$) encompasses a small range of scattering angles ($\theta < 3^{\circ}$), so that the Ewald sphere can be approximated as an Ewald plane, $(q_{||}, q_{\perp})$, which is normal to the beam, with z along the director n orientation. SAXS and WAXS images of 2N, 7N, and their mixtures with DIO, obtained on cooling from the isotropic to the LC phases, show the intense, diffuse scattering features at $q_{||} \sim 0.25$ \mathring{A}^{-1} and $q_{\perp} \sim 1.4 \mathring{A}^{-1}$ from end-to-end and side-by-side molecular positional pair correlations, respectively, that are characteristic of this type of polar mesogen.

Electro-optics. For making electro-optical measurements, the mixtures were filled into planar-aligned, in-plane-switching test cells with unidirectionally buffed alignment layers on both plates. Cells with antiparallel buffing on plates separated by $d=3.5~\mu m$ and with parallel buffing on plates with a $d=5~\mu m$ separation were used. The two in-plane ITO electrodes were spaced by 1 mm and otherwise covered most of the 1 cm² glass plate of the cell. The buffing was parallel to the electrode gap. Such surfaces give a quadrupolar alignment of the N and SmZ_A directors along the buffing axis and polar alignment of the N_F at each plate. Antiparallel buffing stabilizes a twisted configuration in the N_F phase, generating a director/polarization field that is parallel to the plates and undergoes a π twist between them (10). Parallel buffing generates polar monodomains in the N_F and SmA_F phases.

Data, Materials, and Software Availability. Data and videos have been deposited in the Open Science Framework (OSF) at https://osf.io/PFTGR, (41).

ACKNOWLEDGMENTS. This work was supported by NSF Condensed Matter Physics grants DMR-1710711 and DMR-2005170, by Materials Research Science and Engineering Center (MRSEC) grant DMR-1420736, by University of Colorado Lab Venture Challenge Office of Economic Development and International Trade grant APP-354288, and by Polaris Electro-Optics. This research used the microfocus Soft Matter Interfaces beamline 12-ID of the NSLS II, a US Department of Energy (DOE) Office of Science User Facility operated for the DOE Office of Science by Brookhaven National Laboratory under contract No. DE-SC0012704. X-ray experiments were also performed in the Materials Research X-Ray Diffraction Facility at the University of Colorado Boulder (RRID: SCR_019304), with instrumentation supported by NSF MRSEC grant DMR-1420736.

Author affiliations: ^aDepartment of Physics and Soft Materials Research Center, University of Colorado Boulder, Boulder, CO 80309; ^bInstitute of Physical Chemistry, University of Stuttgart, 70569 Stuttgart, Germany; 'Department of Chemistry and Soft Materials Research Center, University of Colorado Boulder, Boulder, CO 80309; ^dElectronics Division, Merck KGaA, 64293 Darmstadt, Germany; and ^eNational Synchrotron Light Source-II, Brookhaven National Laboratory, Upton, NY 11973

- 5. N. Sebastián et al., Ferroelectric-ferroelastic phase transition in a nematic liquid crystal. Phys. Rev. Lett. 124, 037801 (2020).
- H. Nishikawa et al., A fluid liquid-crystal material with highly polar order. Adv. Mater. 29, 1702354
- X. Chen et al., First-principles experimental demonstration of ferroelectricity in a thermotropic nematic liquid crystal: Polar domains and striking electro-optics. Proc. Natl. Acad. Sci. U.S.A. 117, 14021-14031 (2020)

- J. Li et al., Development of ferroelectric nematic fluids with giant-ε dielectricity and nonlinear optical properties. Sci. Adv. 7, eabf5047 (2021).
- X. Chen et al., Ideal mixing of paraelectric and ferroelectric nematic phases in liquid crystals of distinct molecular species. Liq. Cryst. 49, 1531–1544 (2022).
- X. Chen et al., Polar in-plane surface orientation of a ferroelectric nematic liquid crystal: Polar monodomains and twisted state electro-optics. arXiv [Preprint] (2020). doi.org/10.48550/arXiv. 2012.15335. Accessed 26 October 2022.
- X. Chen et al., Polar in-plane surface orientation of a ferroelectric nematic liquid crystal: Polar monodomains and twisted state electro-optics. Proc. Natl. Acad. Sci. U.S.A. 118, e2104092118 (2021)
- H. Nishikawa, F. Araoka, A new class of chiral nematic phase with helical polar order. Adv. Mater. 33, e2101305 (2021).
- X. Zhao et al., Spontaneous helielectric nematic liquid crystals: Electric analog to helimagnets. Proc. Natl. Acad. Sci. U.S.A. 118, e2111101118 (2021).
- C. Feng et al., Electrically tunable reflection color of chiral ferroelectric nematic liquid crystals. Adv. Opt. Mater. 9, 2101230 (2021).
- R. J. Mandle, S. J. Cowling, J. W. Goodby, Structural variants of RM734 in the design of splay nematic materials. *Liq. Cryst.* 48, 1780–1790 (2021).
- X. Chen et al., Antiferroelectric smectic ordering as a prelude to the ferroelectric nematic: Introducing the smectic Z_A phase. arXiv [Preprint] (2021). doi.org/10.48550/arXiv.2112.14222. Accessed 26 October 2022.
- X. Chen et al., L. Radzihovsky and others, "Observation of a uniaxial ferroelectric smectic A phase. arXiv [Preprint] (2022). doi.org/10.48550/arXiv.2206.12965. Accessed 26 October 2022.
- X. Chen et al., "A uniaxial ferroelectric smectic A phase and the smectic A to smectic Z phase transition" in Presentation IL-4-G, International Liquid Crystal Conference (Lisbon, Portugal, 2022, July).
- F. Hardouin, A. M. Levelut, M. F. Achard, G. Sigaud, Polymorphisme des substances mesogenes a molecules polaires. J. de Chimie Physique et de Physico-Chimie Biologique 80, 53-64 (1983).
- G. Sigaud, N. H. Tinh, F. Hardouin, H. Gasparoux, Occurrence of reentrant nematic and reentrant smectic A phases in mesogenic series. Mol. Cryst. Liq. Cryst. (Phila. Pa.) 69, 81–102 (1981).
- P. G. de Gennes, J. Prost, The Physics of Liquid Crystals (Clarendon Press Oxford, ed. 2, 1993). Ch. 10. ISBN: 9780198517856
- R. Dąbrowski, From the discovery of the partially bilayer smectic A phase to blue phases in polar liquid crystals. *Liq. Cryst.* 42, 783-818 (2015).
- F. Tournilhac, L. M. Blinov, J. Simon, S. V. Yablonsky, Ferroelectric liquid crystals from achiral molecules. Nature 359, 621-623 (1992).
- L. M. Blinov, T. A. Lobko, B. I. Ostrovskii, S. N. Sulianov, F. G. Tournilhac, Smectic layering in polyphilic liquid crystals: X-ray diffraction and infra-red dichroism study. J. Phys. II France 3, 1121–1139 (1993).

- Y. Shi, F. G. Tournilhac, S. Kumar, Bilayer smectic order in a mixture of polyphilic liquid crystals. Phys. Rev. E 55, 4382-4385 (1997).
- S. Śreenilayam, Yu. P. Panarin, J. K. Vij, A. Lehmann, C. Tschierske, Occurrence of five different orthogonal smectic phases in a bent-core (BC) liquid crystal. *Mol. Cryst. Liq. Cryst. (Phila. Pa.)* 610, 116–121 (2015).
- H. Takezoe, Polar liquid crystals ferro, antiferro, banana, and columnar –. Mol. Cryst. Liq. Cryst. (Phila. Pa.) 646, 46–65 (2017).
- A. Jákli, O. D. Lavrentovich, J. V. Selinger, Physics of liquid crystals of bent-shaped molecules. Rev. Mod. Phys. 90, 045004 (2018).
- P. Nacke, A. Manabe, M. Klasen-Memmer, M. Bremer, F. Giesselmann, "New example of a ferroelectric nematic phase material, Poster P2" in 18th International Conference on Ferroelectric Liquid Crystals: Polarity and Chirality in Soft Matter (Ljubljana, Slovenia, 2021, September).
- N. Sebastian, R. J. Mandle, A. Petelin, A. Eremin, A. Mertelj, Electrooptics of mm-scale polar domains in the ferroelectric splay nematic phase. *Liq. Cryst.* 48, 2055–2071 (2021).
- I. Dozov, G. Durand, Quantized grain boundaries in bent smectic-A liquid crystal. Europhys. Lett. 28, 25–30 (1994).
- Z. Zhuang, J. E. Maclennan, N. A. Clark, Device applications of ferroelectric liquid crystals: Importance of polarization charge interactions. *Proc. Soc. Photo Opt. Instrum. Eng.* 1080, 110–114 (1989).
- C. S. Rosenblatt, R. Pindak, N. A. Clark, R. B. Meyer, Parabolic focal conic defects in the smectic a phase. J. Phys. (Paris) 38, 1105–1115 (1977).
- H. Kikuchi et al., Fluid layered ferroelectrics with global C_{∞ν} symmetry. Adv. Sci. 9, 2202048 (2022).
- J. O. Indekeu, A. N. Berker, Quadruple reentrance (nematic-smectic-A_d-nematic-smectic-A_d-nematic-smectic-A_d) from the frustrated spin-gas model of liquid crystals. *Phys. Rev. A Gen. Phys.* 33, 1158–1162 (1986).
- J. O. Indekeu, Molecular tail lengths, dipole pairings, and multiple reentrance mechanisms of liquid crystals. *Physica* **140A**, 368–375 (1986).
- J. O. Indekeu, A. N. Berker, Molecular structure and reentrant phases in polar liquid crystals. J. Phys. (Paris) 49, 353–362 (1988).
- A. N. Berker, J. S. Walker, Frustrated spin-gas model for doubly reentrant liquid crystals. Phys. Rev. Lett. 47, 1469-1472 (1981).
- N. V. Madhusudana, Simple molecular model for ferroelectric nematic liquid crystals exhibited by small rodlike mesogens. Phys. Rev. E 104, 014704 (2021).
- P. Kirsch et al., Super-fluorinated liquid crystals: Towards the limits of polarity. Eur. J. Org. Chem. 2008, 3479–3487 (2008).
- M. A. Glaser, J. E. MacLennan, X. Chen, Ferroelectric smectic A. OSF. https://osf.io/PFTGR/. Deposited 11 June 2022.